Science of the Total Environment xxx (xxxx) xxx

Contents lists available at ScienceDirect

Science of the Total Environment

journal homepage: www.elsevier.com/locate/scitotenv

Research Paper

Simulating the effect of check dam collapse in a debris-flow channel

Tommaso Baggio *, Vincenzo D'Agostino

Department of Land, Environment, Agriculture and Forestry, University of Padova, viale dell'Università 16, 35020 Legnaro, PD, Italy

HIGHLIGHTS

- Erosion and deposition in a debris-flow event with check dam collapses are analysed.
- A new methodology is proposed to model the effect of check dam collapse.
- When check dams break debris-flow volume increases due to bed erosion at the most.

GRAPHICAL ABSTRACT

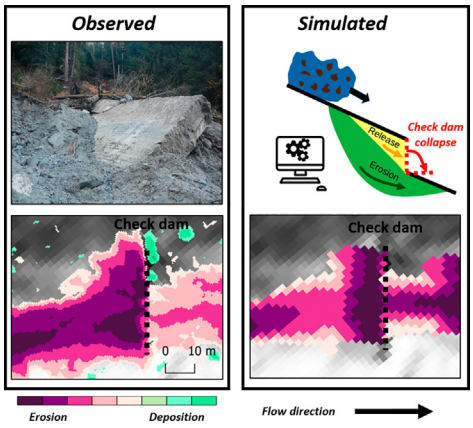

ARTICLE INFO

Article history:
Received 5 August 2021
Received in revised form 9 November 2021
Accepted 9 November 2021
Available online xxxx

Editor: Fernando A.L. Pacheco

Keywords:
Debris flow
Check dam collapse
Bed erosion
Propagation modelling

ABSTRACT

Sequences of erosion control/consolidation check dams are the most widespread channel countermeasure in the European Alps. Some of them were built in the past based on ancient technologies. Nowadays they may not be fully adequate to mitigate the debris-flow/flood events that are becoming more frequent and intense. Consequently, there is the remote possibility that they could fail with disastrous consequences as observed in some cases. A reliable methodology to reproduce the effect of check dam collapse has not yet proposed. Therefore the aim of this study is to define a procedure to simulate the effect of check dam collapse in a debris-flow event. In this study we analysed the catastrophic debris flow occurred in the Rotian channel (Italian Alps) during which a series of check dams collapsed magnifying the event and causing severe damages.

With the aid of field data we reconstructed the event and used the simulation tool r.avaflow to reproduce the debris flow. We then defined three scenarios to simulate the event: (A) debris-flow propagation over an erodible channel; (B) propagation on a rigid channel bed combined with the release of impulsive masses to isolate the analysis of the effect of check dam collapse; (C) a combination of the previous scenarios. The simulation performance was assessed analysing the pre- and post-event LiDAR surveys.

Results showed that the C scenario accurately reproduced the observed debris-flow erosion pattern. In particular, we found out that most of the entrained debris volume derived from bed erosion rather than the sediment retained by check dams. The adopted method, which composes the contribution of bed erosion and check dam collapse, could be of particular relevance for residual risk estimation when mitigation structures are old and may fail with potential disastrous consequences.

* Corresponding author.
E-mail address: tommaso.baggio@phd.unipd.it (T. Baggio).

https://doi.org/10.1016/j.scitotenv.2021.151660
0048-9697/

Please cite this article as: T. Baggio and V. D'Agostino, Simulating the effect of check dam collapse in a debris-flow channel, Science of the Total Environment, https://doi.org/10.1016/j.scitotenv.2021.151660

1. Introduction

Debris flows are rapid mass movements made up by a mixture of water, fine particles, sediment and boulders (Hungr et al., 2014; Jakob et al., 2005; Takahashi, 2007). They can develop high velocities (up to 10 ms^{-1}) generating impressive impact forces (Rickenmann et al., 2003) because of their high bulk density. When debris flows affect villages they can completely destroy infrastructures and buildings causing severe damage and fatalities (Dowling and Santi, 2014; Larsen et al., 2001). For this reason, debris-flow mitigation structures have been built to reduce the associated risk. Such structures mitigate the risk in different ways (Huebl and Fiebiger, 2005; Mizuyama, 2008): they decrease the flow velocity and bed erosion rates (consolidation check dams), promote sediment deposition (flow breakers, open retention check dams, sediment traps, deposition areas, flood reservoir), prevent bed and bank erosion (channelization, bank reinforcements, bed sills) and control the flow spread (deflection walls). Such countermeasures are planned and located according to the morphology, sediment budget and characteristics of the channel and basin (Johnson and McCuen, 1989; Osti and Egashira, 2008). All of these structures have the final goal of reducing the potential consequences of debris-flow events. The hazard and risk map is calculated taking into account the mitigation structures located in the watershed (Fuchs et al., 2007; Gentile et al., 2007; Rodríguez-Morata et al., 2019). A consolidation check dam is the most common type of mitigation structure for debris flow within the channel bed (Piton and Recking, 2014). They are transversal structures often built in a staircase – like sequence in a way that decreases bed erosion, sediment transport, front velocity, pulse behaviour and bank destabilization (Zeng et al., 2009). Even if check dams have been designed taking into account the geomorphological conditions after analysing past events, they may not be representative of future events (Hübl et al., 2005). In fact, in the last decades climate change has rapidly triggered glacier melting, permafrost degradation and taken rainstorms to extremes (Borga et al., 2014; Prein et al., 2016; Stoffel et al., 2014; Vagnon, 2020). The expected consequence is an increase of debris-flow severity and frequency in terms of water and sediment volume. Moreover, check dams can be damaged by debris flow and debris flood over decades, causing scouring erosion to the foundations, damage to the crest and body and lateral erosion (Tacnet et al., 2012; Victoriano et al., 2018). Furthermore the correct maintenance of mitigation structures is increasingly lacking (Mazzorana et al., 2014). The consequences may lead to the collapse of check dams as observed in some cases of extreme events (Benito et al., 1998; Chen et al., 2015; Cucchiaro et al., 2019a, 2019b; Wang, 2013). The volume of debris flow increases both because of the released material during the collapse and the increase of local channel slope after the collapse (Piton et al., 2016). As consequence of channel slope increase both entrainment (Gregoretti, 2008; Lamb et al., 2008) and transport capacity (Armanini, 2015; Lanzoni et al., 2017; Takahashi, 2007) grow. Therefore the failure of a check dam or a series of them can have incredibly severe consequences, and debris flows can likely impact areas classified as having no or low risk. Then, the concept that mitigation measures are commonly always considered adequate to decrease the event magnitude may not be totally confirmed (Piton et al., 2016). Scenarios of mitigation structures collapse are seldom considered but they should at least be mentioned and taken into account as a remote but possible scenario in the risk assessment framework.

Simulation tools can reproduce the dynamic of mass movements (landslides, debris flows, floods) along a defined topography given a set of input data (Scheidl et al., 2013). Therefore, the production of hazard maps and then risk maps is commonly based on the output of hydraulic and mass flow propagation models (Mazzorana et al., 2009; Stecher et al., 2012). Simulation tools can be used to assess the effectiveness of check dams (Bernard et al., 2019; Osti and Egashira, 2008; Remaître et al., 2008; Liu et al., 2012) and to predict the residual risk in the case of protection measure collapse (Tseng et al., 2012). To simulate structure collapse scenarios, the choice of an adequate simulation tool is fundamental to reproduce the phenomena in the most reliable way. For debris flow phenomena the tool should match different characteristics. (i) It should consider the flow as a biphasic mass in order to both accurately represent the behaviour of the debris flow phenomenon (Kean et al., 2013) and to reproduce the released or entrained mass since they are characterized by a higher debris content than the flowing mass (Papa et al., 2004). (ii) The model should incorporate the flow propagation over erodible bed, since erosion processes can be really strong after the structure collapse (Cucchiaro et al., 2019a). (iii) The simulation tool should consider (a) the possibility of introducing the volume into the computational domain through mass release to represent the volume of debris released after the check dam collapse and (b) a solid-liquid hydrograph to introduce the debris-flow routing. Different models for debris-flow propagation have been developed in the last years and successfully tested with real case scenarios (Frank et al., 2015; Gregoretti et al., 2018; McDougall and Hungr, 2004; O'Brien et al., 1993; Rosatti and Begnudelli, 2013). Some of them incorporate an erosion model and the possibility of releasing a mass. Among the different tools, r.avaflow (Mergili and Pudasaini, 2021) resulted adequate for structures collapse scenarios thanks to its flexibility in introducing the mass in the computational domain, the presence of the empirical erosion model (Mergili et al., 2017) and the multi-phase mass flow propagation model (Pudasaini and Mergili, 2019). Moreover, r.avaflow have already been used to back calculate geomorphologically complex scenarios that include interaction between landslide, glacier, debris flow and lake (Baggio et al., 2018; Gylfadóttir et al., 2019; Mergili et al., 2020b, 2018). The empirical erosion model has been analysed and calibrated for landslide (Mergili et al., 2020a) and debris flow phenomena (Baggio et al., 2021).

The need to strengthen our capacity to model the effect of the collapse of a series of check dams is still an open research question (Zhang et al., 2019) and is motivated by the increasing attention of public authorities towards communication of the residual hazard and related risk (Hartmann et al., 2021). The aim of this study is to develop and test a procedure to adequately simulate the effect of check dam collapse in case of a high-magnitude debris-flow event.

For this purpose a recent extreme debris-flow event amplified by the failure of a series of check dams is presented. Thanks to pre- and post-event surveys and a field campaign, the event is reconstructed. The debris-flow hydrograph is estimated and an operative procedure is proposed to simulate the effect of check dam failure. Three simulation scenarios are computed to reproduce the effects of check dam failure through mass release and channel erosion. The following discussion considers the reliability, implications and generalization of the results. The outcomes of the study highlight a replicable methodologic path that can be used to simulate the consequences of check dam failure in debris-flow hazard scenarios for risk mapping.

2. Material and methods

In this section it is first described the characteristics of the Rio Rotian catchment reporting the morphology of the channel, the pre-event mitigation structures and fan description. Then, the debris-flow event occurred on 29th October 2018 is recounted, describing the methods to reconstruct the debris-flow characteristics and erosion pattern. Lastly, the simulation model is depicted, as well as the input data to reproduce the event and evaluate the simulation performance.

2.1. Study site: the rio Rotian channel

The rio Rotian channel is a mountainous torrent located in the autonomous province of Trento, in the Eastern Italian Alps. The catchment has a total extent of 2.4 km^2 and a mean slope of 26.4°, extending from an altitude of 2042 to 824 m a.s.l. (Fig. 1). The shape of the basin is elongated along the main channel path in a north – east direction. The

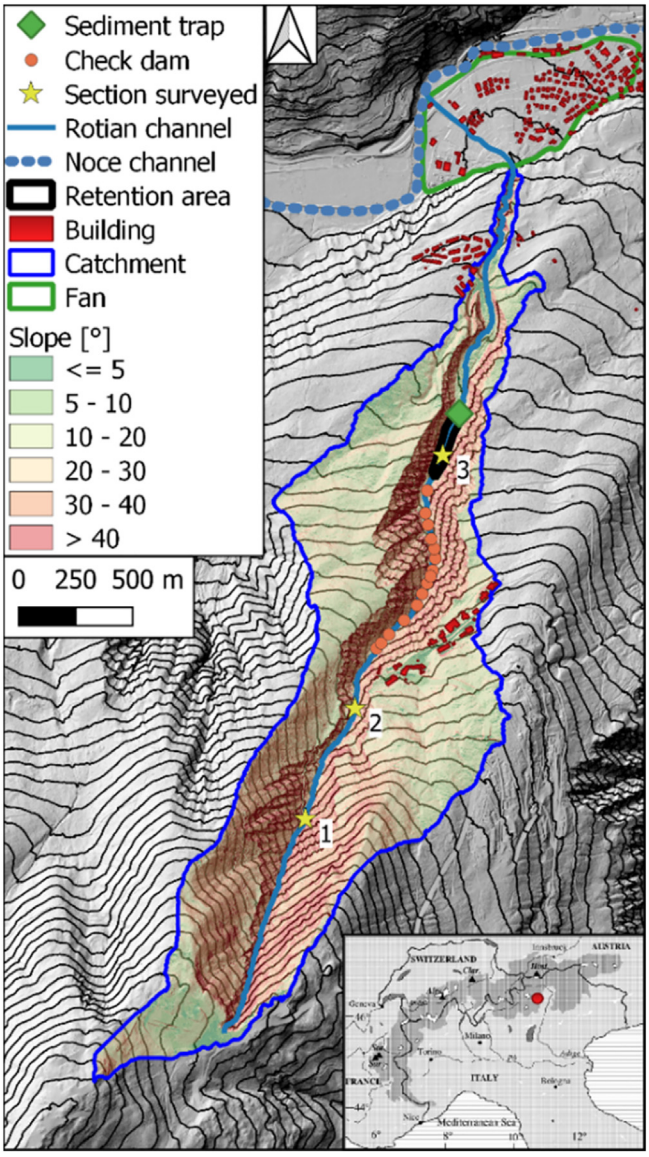

Fig. 1. Overview of the rio Rotian catchment and fan, showing the position of mitigation measures and the surveyed sections. In background the slope map. (contour lines altitude difference: 25 m).

geology of the basin is composed by colluvial, alluvial and glacial deposits in the lower part (below 1300 m a.s.l.), while the upper part is composed by stratified layers of limestone and clay. Due to these geological characteristics, in the last centuries the channel progressively deepened, generating a canyon-like incision of around 10–50 m of elevation difference compared with the top of the banks. The banks are very steep (range 30–45°) and they are very probably the source of sediment supply to the stream in the case of intense runoff.

The channel is 4.8 km long and has a mean slope of 11.9°. It has been consolidated with a series of 15 check dams built in 1977 (reach in the range from 1233 to 1030 m a.s.l.) and made of reinforced concrete. The check dam mean height is 5.3 m (range 2.9–7.8 m) for a cumulative sum of 78.9 m and a mean channel slope of 13°. Immediately downstream of the last check dam the channel bed has been enlarged in order to create a depositional area formed by a series of 5 retention basins connected each other by a sloped reach (total length 250 m, mean width 25 m). In 2014, a 7.4 m high open check dam was constructed at 989 m a.s.l., immediately downstream of the retention basins (Fig. 1), to increase the deposition of the flowing solid component.

The fan apex is at an altitude of 824 m a.s.l. and the fan has an area of 0.38 km^2. The channel crosses the fan centrally and joins with the Noce river at an elevation of 782 m a.s.l. The village of Dimaro is located on the fan, mainly consisting of a campsite on the left hand side of the channel and settlements on the right hand side.

In the past, the Rotian channel produced three recorded debris-flow events. The 1776 event was described as a catastrophic phenomenon: the channel transported a large amount of sediment to the confluence with the Noce river stopping the flow and deviating its original path. In 1882 two debris-flow events of the same magnitude hit the village destroying some settlements and depositing boulders in the fan area. More recently, in September 2000, the Rotian channel produced a small debris-flood event where most of the transported sediment was deposited upstream of the fan apex and the flow remained confined to the channel path.

2.2. The 27-30th October 2018 event

Between the 27th and 30th October 2018 the North-Eastern Italian Alps were hit by an extreme storm, named "Vaia". The event was characterized by intense rainfall associated with high wind speeds, up to 200 km h^{-1} (Chirici et al., 2019). Focusing on the rio Rotian basin, the debris flow occurred at the end of the Vaia storm on the 29th October. The event was characterized by three different surges occurring at 19:02, 19:48 and 23:35 CET (Borga and Zaramella, 2020). An analysis of the rainstorm was carried out by Borga and Zaramella (2020) using the radar data of the Macaion station (located 32 km in the NE direction with respect to the fan apex). They calculated a total precipitation amount of 359 mm for the rio Rotian basin in the period 27 – 29th October, corresponding to a return period (three days maximum) of 300 years. Furthermore, the most intense precipitation occurred at the end of the event. A further rainfall analysis on the duration of the 3 h before the event resulted in a return period of 100 years (Borga and Zaramella, 2020). The basin, already stressed by two consecutive days of heavy rainfall, generated a catastrophic debris flow. The flow was characterized by major bed destabilization and erosion, which took place starting from the upper part of the basin. Propagating downward the flow increased its sediment component and destroyed the series of 15 check dams. The collapsed structures released debris that was engulfed by the flow causing a further bed instability and triggering a severe erosion process. The open check dam situated at 989 m a.s.l. retained a large quantity of the transported debris (32,000 m^3) but its storage capacity was not sufficient to effectively reduce the debris volume of such an extreme event. Consequently, the debris flow continued propagating downwards and flooded part of the fan, depositing a large volume of debris along the roads of the village (160,000 m^3). The flow affected several settlements and the campsite, causing severe damage and one fatality.

The debris flow was mainly formed by a fine sediment matrix (principally silt and sand) together with large rocks and boulders. According to field evidence, the debris flow can be classified as a muddy debris flow (Jakob et al., 2005). The front of the debris flow transported big boulders (diameters larger than 1 m and up to 6 m) depositing some of them in the fan, near the campsite (Fig. 2A). A really big boulder (estimated volume of 18 m^3) was transported probably by the front of the flow and completely closed the open check dam (Fig. 2B). Parts of the collapsed check dams were entrained in the flow and pieces were found in the retention basins (Fig. 2C). In addition, the channel part upstream of the 15 consolidation check dams exhibited erosion and bank destabilization (Fig. 2D).

Two days after the event (31st October 2018) the Mountain Basin Service of the Trento province performed a drone survey involving the fan area. Seven days later (7th November 2018) the Service surveyed the channel in the zone of the sediment trap and retention basin (1050 m a.s.l.), covering a torrent length of 350 m upstream of the check dam. Fifteen ground control points (GCP) were located within

Fig. 2. Pictures of the post-event conditions. The debris deposit at the campsite (A), the sediment trap (B), the check dam channel reach (C) and the upper part of the channel (D); the white and red lines represent the minimum and maximum debris-flow front height with respect to the channel bed.

the surveyed area and their positions recorded with a high resolution GPS (estimated error of 0.05 m). The acquired images were processed to generate a point dense cloud and then a high resolution (0.1 m) digital surface model (Basin Mountain Service, 2018). Regarding the upper part of the channel that was not surveyed with the drone flight, we used the 2019 LiDAR data (acquired on 14-15th June 2019 with a 0.5 m resolution) as representative of the post-event conditions (no debris flood and flow events occurred between the October 2018 event and the LiDAR survey). Thanks to the pre-event LiDAR survey (acquired in 2014, 0.5 m resolution, error 0.1 m) we then performed a Dem of Difference (DoD) analysis, calculating the eroded and deposited volume pattern for the whole channel path and fan area. We used the minimum level of detection method (Brasington et al., 2003) to estimate the associated error. The DoD error is the result of the following equation $\delta u_{DoD} = \sqrt{\delta u_{pre}^2 + \delta u_{post}^2}$, where δu_{pre} and δu_{post} are the pre- and post-event associated DTM errors, respectively. The DoD analysis was the basis for the event reconstruction, input hydrograph, magnitude estimation and evaluation of the simulation performance.

On the 12th and 13th November we collected field data walking along the channel bed from the confluence with the Noce river to an elevation of 1480 m a.s.l. The grain-size distribution of the debris for three different sampling points was collected (two in the channel path and one in the retention basin). Also three channel sections were acquired in places where the estimated channel erosion was weak and where the maximum flow level was recognizable on both banks. For every section the upward thalweg profile was surveyed for a minimum distance of 25 m. The profiles and sections were surveyed measuring the horizontal and vertical distance with a TruePulse laser distance meter (accuracy 0.1 m). The maximum flow depth (sign of the passage on the banks), flow area and upward thalweg slope were derived. Empirical equations reported in the literature were used to back calculate the peak flow velocity v (Hungr et al., 1984; Lo, 2000; Prochaska et al., 2008; Rickenmann, 1999) and consequently the peak discharge. The general form of velocity [m/s] empirical equation is $v = a(H^b S^c) + d$ where H is the flow depth [m], S the thalweg slope [m/m] and a, b, c, d are empirical coefficients reported in Table 1. The calculated peak discharge was compared with the empirical equation of Benini (2000),

Table 1
discharge peak reconstruction of the surveyed sections through empirical equations derived from field data. The suffix "mod" means that the surveyed max flow depth has been modified. We also report the empirical equations to calculate the max flow velocity and the peak discharge.

Section ID	Max flow depth [m]	Wet area [m^2]	Slope [m m^1]	Velocity [m/s]				Peak discharge [m^3/s]				
				Hungr et al. (1984)	Lo (2000)	Rickenmann (1999) & Lo (2000)	Rickenmann (1999)	Hungr et al. (1984)	Lo (2000)	Rickenmann (1999) & Lo (2000)	Rickenmann (1999)	*Mean*
				$v = 0.55H^{3/2} S^{1/2} + 4.59$	$v = 3.32H^{2/3} S^{1/5} + 0.70$	$v = 4.47H^{2/3} S^{1/2} + 1.71$	$v = 8.90H^{0.30} S^{1/2} + 1.06$	Velocity x Wet area				
SEZ. 1	3.3	25.4	0.41	6.7	5.4	8.0	8.6	169.3	136.7	203.6	218.3	187.0
SEZ. 1 mod	1.8	15.8	0.41	5.4	3.8	5.9	6.6	85.2	59.7	92.5	103.5	78.3
SEZ. 2	3.5	46.5	0.20	6.2	4.1	6.3	6.4	287.9	190.5	292.2	300.0	267.6
SEZ. 3	8.3	237.4	0.17	9.9	6.2	9.2	8.7	2354.4	1481.4	2176.8	2064.4	2019.3
SEZ. 3 mod	5.8	82.6	0.17	7.7	5.1	7.6	7.5	638.8	419.8	628.6	616.2	575.9

which considers the threshold for motion velocity of a sediment particle transported by a debris flow (in this case we considered the maximum particle diameter D that was moved):

$$v = \left[21.8\frac{(\gamma_s - \gamma)}{\gamma}\right]^{0.5} D^{0.5} \quad (1)$$

where γ_s and γ are the specific weights of the particle and flow, respectively.

Using the DoD map the erosion upstream section 1 (Fig. 1) was derived to calculate the debris volume. For further verification, the obtained value is compared with empirical relationships (Mizuyama et al., 1992).

Based on the peak discharge and total solid volume estimation, for a modelling aim an input hydrograph with a triangular shape was derived, fixing the volumetric concentration of the solid component to 0.5 (Gregoretti et al., 2018).

2.3. Simulation model and input data

To back calculate the debris flow, the simulation tool r.avaflow version 2.4 was adopted (Mergili and Pudasaini, 2021). The tool implements the multi-phase mass flow model described in Pudasaini and Mergili (2019). The model can simulate the propagation of different types of mass flows down a general topography. The mass can be introduced in the calculation domain simultaneously or alternatively through a hydrograph (discharge versus time relation) or a release mass (raster map). An additional function of the model is the possibility of releasing the mass from a certain cell at a given time.

Implementing r.avaflow for the Rotian debris-flow event, the multi-phase model was reduced to a two-phase model, considering the solid component as debris material and the fluid one as water. The selected flow parameters are basically the same values reported in the user manual (Mergili and Pudasaini, 2021). We varied two flow parameters in order to reproduce the rheology of a muddy debris flow. In particular, the basal friction angle was decreased to 16° and the fluid kinematic viscosity was increased to 0.005 m^2s^{-1}. Furthermore, the tool provides an empirical multi-phase erosion model, calculating for each time step (Δt) the entrained volume in terms of erosive depths D_E by means of the following function of the flow momentum (M) (Eqs. (2) and (3)):

$$D_{E,s} = C_E|M_s + M_f|\alpha_{s,Emax}\Delta t \quad (2)$$

$$D_{E,f} = C_E|M_s + M_f|(1-\alpha_{s,Emax})\Delta t \quad (3)$$

where C_E is the coefficient of erosion, $\alpha_{s,Emax}$ the sediment volumetric concentration of the eroded material and M is the flow momentum. The subscripts s and f refer to the solid and fluid phase of the flow, respectively.

The erosion model requires the assignment of C_E, $D_{E,max}$ maximum erosion depth, and $\alpha_{s,Emax}$. These parameters are defined by the user alternatively as a single value or spatially distributed (raster map). The maximum erosion depth was set to 10 m (maximum erosion observed) but erosion was not permitted in correspondence to the retention basin and sediment trap, since in those locations the channel bed was reinforced with stones. Indeed, $\alpha_{s,Emax}$ was set to 0.7, representing the water saturated pre-event soil conditions. The value is similar to that observed in the triggering area of two debris-flow basins of Eastern Alps (Gregoretti et al., 2019, 2018). Deposition is considered as the remaining mass at the end of the simulation time; in this study it is fixed to 3000 s (50 min) for all simulations performed.

Regarding the DTM, the 2014 LiDAR derived terrain model was used, representing the pre-event conditions. The original DTM was resampled from a resolution of 0.5 m to 2 m for computational speed, adopting a mean value method. The DTM was further modified to represent the open check dam, since it was under construction in 2014. It has been represented as a rigid wall since the opening had been closed by a big boulder, likely transported by the front of the debris flow. We located the input hydrograph 830 m upstream of the first check dam in correspondence to the surveyed section 1 (Fig. 1).

To reproduce the Rotian debris flow three scenarios, representing three different ways to implement the check dam collapse, were tested:

A. Scenario representing the propagation of the debris flow over an erodible channel bed (check dams are considered erodible). C_E is a function of a smoothed slope (S_S [%], calculated as the mean value within a circular moving window of 5 × 5 cells) as the most performing function calibrated in (Baggio et al., 2021) for debris-flow entrainment over erodible channel.

$$C_{E,exp6} = 10^{(0.02S_s - 6.75)} \quad (4)$$

Moreover, the smoothed slope dependent function was varied in the channel reach between the input hydrograph location and the check dam 01, hereafter Area 1 (Fig. 4), in order to further improve the reliability of the erosion model. In Area 1 the simulated eroded volumes adopting the function of Eq. (4) resulted considerably higher than the observed one. Other two functions were tested (reported in Baggio et al., 2021) to simulate erosion in Area 1, always based on a smoothed slope:

$$C_{Eexp2} = 10^{(0.025S_s - 7)} \quad (5)$$

$$C_{Eexp3} = 10^{(0.03S_s - 7.5)} \quad (6)$$

B. Scenario of a debris-flow propagation over a non-erodible channel bed. The check dam collapses are reproduced by debris material released for every check dam. To calculate the release volume an upward sliding failure slope of 25° was supposed (angle of repose of debris soaked material; assessed by means of local surveys of terrain

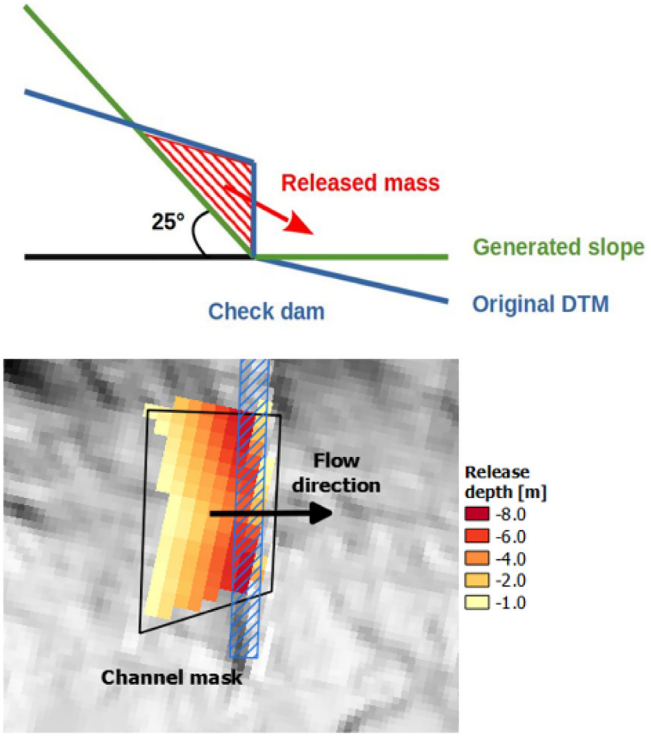

Fig. 3. Profile sketch and plan view of the release depth calculation for the simulation of a check dam collapse.

collapses after the events) as the result of the lack of bed stabilization provided by the check dam Fig. 3. The depth of the released material is then calculated as the difference between the original topography (input DTM) and the assumed failure slope plane. The calculated mass retained by the check dam is released at the passage of the simulated debris-flow peak discharge (estimated with a previous simulation). The solid mass released for every check dam results variable in accordance with its height as highlighted in the sketch of Fig. 3 and the solid ratio has been set to 0.8. Such mass was released considering only the channel bed by means of a mask layer. An example of the final released mass height distribution of a check dam collapse is represented in Fig. 3. The calculation was implemented as a pre-processing algorithm in the same script to launch the mass flow propagation with r.avaflow. The input data required for every check dam is a polyline identifying the downstream border of the check dam step and a mask outlining the upstream channel bed. It is also possible to adapt the algorithm to reproduce a partial collapse of a check dam in terms of height or width. In the first case (height under collapse) it is just necessary to modify the elevation value of the lowest border of the computer generated slope. In the second case (work width under collapse) the channel mask can be modified to simulate the check dam collapse for a particular area of interest.

C. Scenario representing a combination of the previous two scenarios. The mass representing the check dam collapse is calculated and released at the peak discharge passage as explained in B. Moreover, erosion is allowed in the computational domain and C_E has been set to a unique value for the whole computational domain. Six simulations were performed where C_E was progressively varied from 10^{-7} to $10^{-6.2}$ kg^{-1} in order to calibrate the erosion coefficient in accordance with the observed erosion volume of the check dam series in the torrent reach under analysis.

To evaluate the best scenario the observed net balance (difference between deposited and eroded volumes) was compared with those simulated for two selected channel reaches. Area 1 represents the channel reach between the input hydrograph and a section 50 m upstream of check dam 1, while Area 2 encloses the channel part of the check dam series (Fig. 4). In particular, a simulation was considered accurate when it reproduces the balance volume within an error of 20% with respect to the observed value.

3. Results

3.1. Hydrograph reconstruction

Hydrograph reconstruction was based on the calculation of the solid volume (DoD map) and on the peak discharge reconstruction. Adopting empirical relations, the mean velocity was derived for the debris-flow front. Then, the bulked peak discharge was calculated through the product of the wet area surveyed in the field and the flow velocity of the front.

A total of three channel sections and the related upstream channel profile were surveyed, collecting their horizontal and vertical coordinates with respect to a reference point (locations are reported in Fig. 1). The maximum flow depth that occurred during the 29th October 2018 event, the upward thalweg slope and wet area were estimated. Through the empirical equations, the peak discharges were derived, which are listed in Table 1. For section 1 the maximum flow depth was modified, decreasing the value of 1.5 m. In fact, it was assumed that the channel deepening to the bedrock was caused by the tail of the debris flow and not by the front surge under estimation. A sign of such front passage can be identified in the channel banks, (Fig. 2D, white and red lines). The modification of the bed bottom position were supported by information on the bed topography from the DoD map.

The calculation of the peak discharge of section 1 is particularly important, since it is the basis for the construction of the input hydrograph for the simulation model. From Table 1 it is possible to identify the peak discharge of section 1 that for the modified section resulted 78 $m^3 s^{-1}$, calculated as the mean of the empirical equations. The estimated total solid volume from the DoD map resulted 33,600 m^3. The value is computed as the erosion rate per channel length between section 1 and 2 (equal to 32 $m^3 m^{-1}$ according to the DoD) multiplied by the channel length upstream of section 1 (1050 m). The estimation has been performed due to the impossibility to compute a reliable DoD map upstream of section 1 (presence of vegetation cover within the channel and steep slopes not well captured by the post-event survey). Using the equation of Mizuyama et al. (1992) the solid volume associated to the peak discharge of 78 $m^3 s^{-1}$ resulted 37,237 m^3. The statistical analysis of debris flows occurring in the Eastern Alps by Marchi and D'Agostino (2004) corroborated the debris volume of such an event. According to these authors, the maximum debris volume (V_s) related to the upper catchment area A [km^2] is given by the upper envelope equation: $V_s = 70{,}000\,A$, calculating a value of 41,300 m^3 for section 1 (upper catchment area of 0.59 km^2). This value is in line with the debris volume derived from the DoD map upstream of the section 1. Furthermore, the peak discharge in section 1 was confirmed by means of the limiting equation (Eq. (1)) for boulder entrainment (max grain diameter 1.0 m), obtaining a value of 81.6 $m^3 s^{-1}$. The comparison with equations reported in the literature and the DoD analysis confirmed that the calculated peak discharge and associated debris volume can be consistently representative of the investigated event.

We then used these values to build up an input hydrograph with a triangular shape in accordance with field observations (Berti et al., 2000; Gregoretti et al., 2019; Kean et al., 2012). We fixed the peak discharge at 100 s after the hydrograph starts. After the peak, the discharge progressively decreased to zero in a total time of 956 s. The solid volumetric concentration was set to 0.5 since the event was mainly triggered by the movement of the soaked bed deposits within the whole channel path and eye witnesses reported the passage of a dense debris flow.

Regarding the section 2 the estimated peak discharge is equal to 267 m^3/s (mean of all equations). However, this value is probably overestimated since the tail of the debris flow eroded the channel bed increasing the apparent maximum flow depth, that was measured in the field. Besides, the estimated peak discharge of the section 3 was assessed in 575 m^3/s (mean of all equations, Table 1). Also in this case, the discharge assessment is uncertain since a deposition followed by an intense bed erosion influenced maximum flow depth measure.

3.2. Erosional and depositional pattern analysis

The DoD was computed as the difference between the 2019 and 2014 DTM. For our objective, involving the check dam collapse simulation, the focus was on the channel reach between the input hydrograph location (section 1, Fig. 1) and the last downstream check dam (right upstream of the retention basin). Two areas of interest were defined for the calculation of the eroded and deposited volumes (Fig. 4). The error associated with the DoD map resulted 0.14 m and, adopting the minimum level of detection method, the eroded and deposited volumes within the two areas were calculated (Table 2).

In the investigated areas the erosion processes resulted predominant with respect to the depositions one. For Area 1 (comprised between 1435 and 1238 m a.s.l for a length of 817 m) intense erosion was observed, with an associated volume balance per channel length of 31 $m^3 m^{-1}$. In Area 2 (covering the torrent reach between 1238 and 1029 m a.s.l for a length of 852 m) the erosion process became

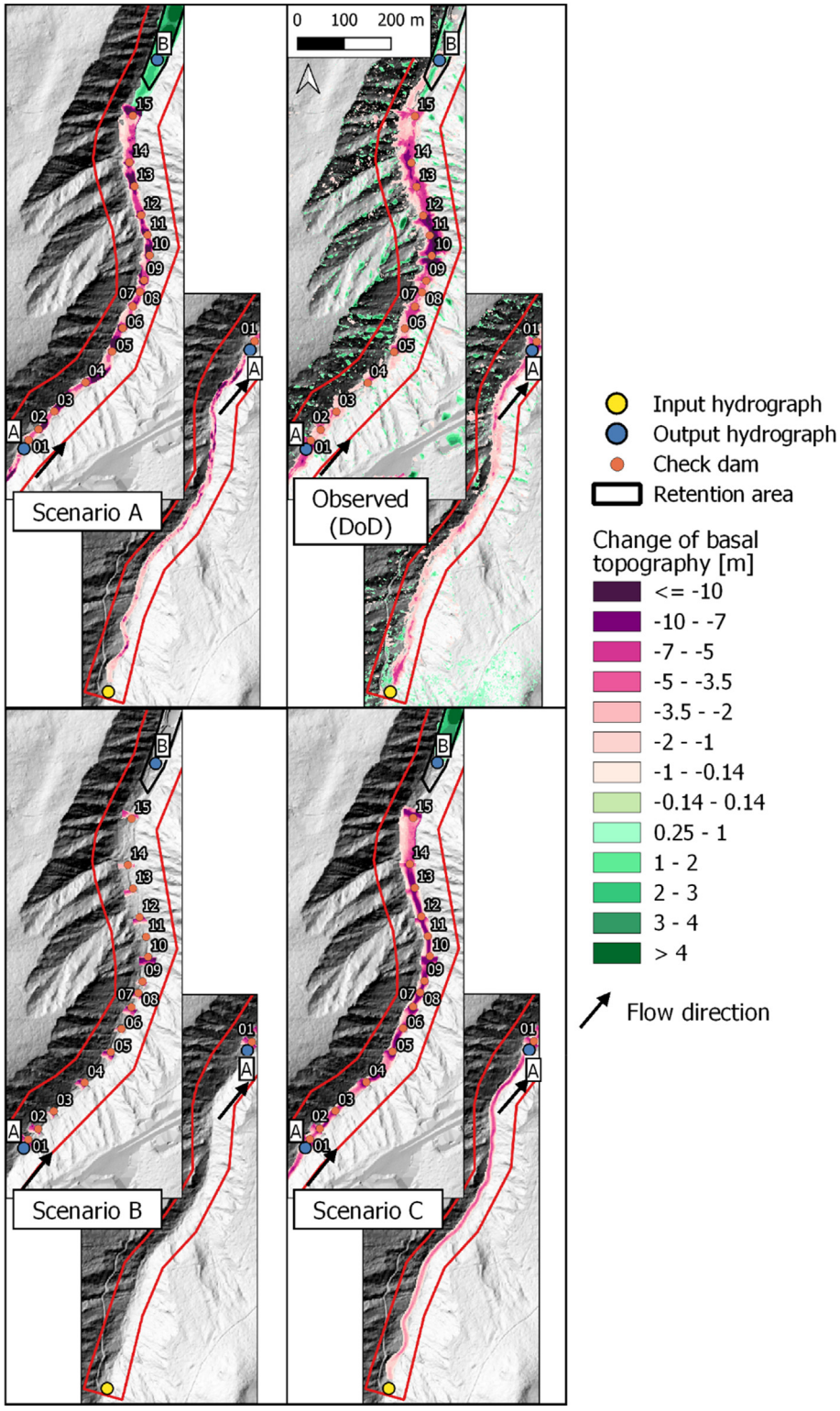

Fig. 4. Maps representing the observed erosion and deposition depths (DoD) and simulated elevation changes respect the basal topography for scenarios A, B and C.

more severe. In this channel segment the erosion resulted 119 m^3m^{-1}. The net balance between eroded and deposited volumes consisted in −25,630 m^3 (± 1855) and 102,393 m^3 (± 4110) for Area 1 and 2 respectively. The erosion depth per channel length in Area 1 is typical of debris-flow triggering reaches, while the high values of Area 2 is the combined result of the check dam collapses and the successive bed erosion process. As to those areas not directly investigated in this study, the volume balance was computed for the zone of the retention basins (from just downstream of Area 2 to the open check, altitude range 1029–989 m a.s.l., length 290 m) resulting in a net balance in favour of deposition of 20,048 m^3 (± 2831). The reach downstream of the open check dam up to the municipal road (altitude range 1029–928 m a.s.l., length 531 m) exhibited erosion processes characterized by a net balance of −18,447 m^3.

Table 2
analysis of the volume balance (deposition – erosion) based on the DoD map and comparison with the simulated scenarios. * Represent the balance error of the DoD for the investigated area.

	Area 1			Area 2		
Scenario	Volume balance (deposited – eroded) [m^3]	Error (simulated /observed)	Volume /channel length [m^3/m]	Volume balance (deposited – eroded) [m^3]	Error (simulated /observed)	Volume/channel length [m^3/m]
Observed	−25,630	1855*	−31.4	−102,393	4110*	−119.2
Scenario A (C_E: Area 1 - > $C_{E,exp2}$; Area 2 - > $C_{E,exp6}$)	−28,732	1.12	−33.72	−99,492	0.98	−116.8
Scenario B (mass release – without erosion)	0	–	0.0	−22,304	0.22	−26.2
Scenario C (mass release and erosion, $C_E = 10^{-6.6.4}$)	−30,864	1.20	−36.2	−109,096	1.07	−128.1

3.3. Scenario results

Three scenarios A, B, C were computed, releasing the selected input hydrograph in section 1. Scenario A involved the flow propagation over an erodible channel, scenario B the release of a mass for every check dam (sketch in Fig. 3) and scenario C was a combination of bed erosion and mass release. The total volume released by the collapse of the check dam series at the passage of the peak discharge is equal to 22,304 m^3 (scenario B and C). The erosion and deposition patterns of the performed simulations are illustrated in Fig. 4. For scenarios A and C were showed only the simulations best matching the observed erosion rates. For scenario A, the best performing simulation is the result of the combination of two C_E functions ($C_{E,exp2}$ for Area 1 and $C_{E,exp6}$ for Area 2, Eqs. (5) and (4) respectively). Regarding scenario C the chosen C_E coefficient is $10^{-6.4}$ kg^{-1}. In Table 2 the comparison between the observed and simulated erosion and deposition volumes is reported. For Area 1, representing the channel reach between the input hydrograph and the first check dam, scenario A performed best, resulting in a relative error of 12% of additional erosion with respect to the observed value. Scenario C predicted a slightly greater volume of eroded sediment volume respect to scenario A with an overestimated error for erosion of about 20%. The simulated erosion patterns of scenarios A and C resulted slightly different in Area 1. In particular, in the scenario A erosion was more variable (more intense for steeper slopes) than in the scenario C for which erosion resulted steadier with a more intense process upstream than check dam 01. Anyway, both scenarios accurately represented the erosion pattern observed in Area 1, since the relative error resulted equal to or lower than 20%. Obviously, in the scenario B no erosion occurred since it has not been permitted in the computational domain. Regarding Area 2, representing the check dam series, both scenarios A and C represented the observed eroded volume satisfactorily and provided a relative error of −2 and 7% respectively. Instead scenario B predicted just a small amount of eroded/released material (22,304 m^3) corresponding to the released debris of the check dam collapses only.

Regarding the erosion pattern in Area 2, we can notice an observed intense erosion process upstream of check dam 01 and between check dam 08 and 11 with associated erosion depths reaching a maximum of 11 m. Moreover, for check dam 06 erosion occurred both upstream and downstream of its position. For check dams 02, 04 and 05 erosion mainly occurred downstream, while for check dams 01 and 03 it occurred mostly upstream. Regarding Area 2 (check dam series), scenario A and C exhibited a similar pattern. Scenario A eroded a large amount of material in correspondence and downstream of the check dams while scenario C generated erosion both upstream and downstream. Even if scenarios A and C are both considered adequate to reproduce the observed eroded pattern, the two simulations have a different approximation in the process representation. The operative procedure developed for scenario C resulted more reliable to simulate the effect of check dam collapse than scenario A, since scenario C released the mass retained by the check dams at the passage of the peak discharge. The hydrograph in Fig. 5B of scenario C captured this aspect of impulsive mass release as highlighted by a greater peak discharge than scenario A.

The output hydrographs reported in Fig. 5 show the discharge (debris and fluid component) and solid concentration variation over time for location A and B highlighted in Fig. 4. In location A scenarios A and C predicted similar maximum discharges, equal to 107 and 121 m^3s^{-1}, respectively. Instead, scenario B produced the same discharge as the input hydrograph (78 m^3s^{-1}), since entrainment was not permitted. Regarding the volumetric solid concentration, scenario A and C showed a stable value around 0.58, while for scenario B it resulted lower, equal to the input hydrograph (0.5, constant for the whole passage of the debris flow). Regarding the output hydrograph in location B, scenario C predicted the highest discharge equal to 99 m^3s^{-1}, while scenario A and B resulted 75 and 43 m^3s^{-1}, respectively. Scenario A and C exhibited a first surge in the front, followed by a higher peak. The discharge of the front surge of scenario C resulted greater than scenario A as consequence of the mass released in the proximity of output location B. The solid concentration pattern showed a higher value in the front (range 0.6–0.65) and it immediately decreased around 0.55 until 17 min of simulation time. Afterward the solid concentration constantly increased to reach values around 1 at the end of the simulation time. This behaviour is the results of the deposition process caused by the open check dam. The biphasic representation of the flow simulated aggradation of the solid component in this area, while the fluid component slowly separated, flowing downstream. The phenomenon is captured by the increase of the solid concentration towards 1.

4. Discussion

In this study the Rio Rotian debris-flow event that occurred on the 29th October 2018 was reconstructed. The peak discharge was first estimated in the triggering area and then three different scenarios were performed using the simulation model r.avaflow, aiming to reproduce the effects of a check dam collapses during the event. The simulation performance were analysed and evaluated using the observed erosion and deposition volumes derived from the DoD map.

The event peak discharge and total volume at section 1 were evaluated with the DoD analysis and confirmed by the equations of Benini (2000) and Marchi and D'Agostino (2004) . Some uncertainties still remain in the estimation of the hydrograph shape due to the impossibility of the discharge time pattern evaluation after the peak passage. However, the choice of a linearly shaped hydrograph is also supported by the observations of two high magnitude debris flows recorded in the triggering area (Simoni et al., 2020). The same pattern has been

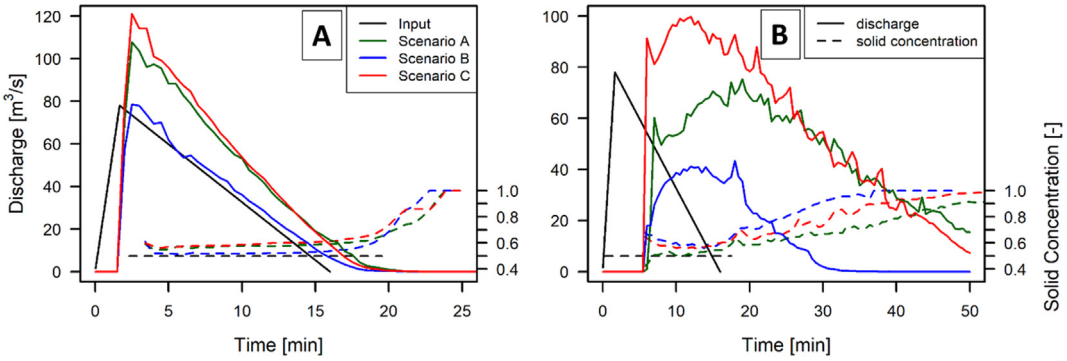

Fig. 5. Output hydrographs for sections A and B (locations are reported in Fig. 4) representing the total discharge (solid + fluid) and solid concentration over time of the simulation scenarios. The input hydrograph is also reported for comparison.

observed in the routing area by Berti et al. (2000) and Kean et al. (2012). In addition, also varying the discharge pattern, the simulation results in terms of erosion may not vary consistently, since the erosion function is strictly dependent on the flow momentum and its highest value occurs in correspondence of the debris-flow front (Berger et al., 2011; McCoy et al., 2012). Regarding section 2 and 3, their geomorphological conditions did not allow a reliable reconstruction of the peak discharge. In section 2, the channel bed erosion process did not permit a reliable estimation of the debris-flow front. Instead, for section 3 the peak discharge evaluation resulted uncertain because of the large amount of debris deposited. Therefore, the estimated peak discharge in section 2 and 3 (Table 1) could not be used for the evaluation of the investigated scenarios.

Regarding the DoD we compared the eroded volumes per channel unit with other observations reported in the literature in order to estimate its magnitude. Regarding Area 1 (natural channel bed) the erosion resulted 31 m^3m^{-1}, which is a high value compared with other studies in the Alps (Marchi and Cavalli, 2007; Marchi and D'Agostino, 2004). For Area 2 (check dam series), erosion resulted 119 m^3 per channel unit length and can be considered as an extreme value for the eastern Alps (Marchi and Cavalli, 2007) and even worldwide (Hungr et al., 2005; Rickenmann and Zimmermann, 1993). However such a high erosion value is the consequence of check dam collapse and is fully comparable, in terms of geomorphological estimation of debris-flow volumes, to that associated to a triggering area. Analysing erosion in Area 2, this occurred predominantly upstream and downstream of the check dam location (Fig. 4). Deposition process started just downstream of check dam 15 where the channel slope becomes gentler due to the presence of the retention basins (mean channel slope of the first deposit equal to 8.4°). More importantly, we observed that: i) the spatially distributed bed erosion is the dominant mechanism in debris-flow entrainment in the case of check dam failure; ii) this erosive pattern is not particularly different from that obtainable in the absence of check dams and it cannot be expected in a particular reach of the torrent (e.g., always downstream of the collapsed work; Fig. 4). In fact, the total eroded volume (102,393 m^3) is around five time greater than the volume estimated and released by the collapse of the 15 check dams (22,304 m^3) reported in scenario B (a sketch for the calculation of the volume released is reported in Fig. 3). Therefore, the principal cause of debris-flow growth is represented by bed erosion as consequence of check dams collapse. A similar phenomenon is reported in Benito et al. (1998), where the collapse of retention dams triggered an extreme debris-flow event in the Biescas basin (Spain). Similarly to the Rotian channel, the Biescas debris flow acquired debris from incision into the unconsolidated glacial deposits after the barrier collapse. A similar mechanism of entrainment is also reported in Chen et al. (2015) and Gong et al. (2020), where the collapsed check dams destabilized the channel bed, permitting an intense bed erosion process.

Regarding the simulations, scenarios A and C successfully reproduced the observed erosion volume of the check dam series (relative error ≤ 20%). In particular, in scenario C a simulation representing the effect of check dam collapse was set up, calibrating an erosion coefficient based on the observed eroded volume. A semiautomatic procedure was developed to derive the spatially distributed volume retained by the check dams. The effect of check dam collapse was then simulated through mass release in the computational domain synchronised with the peak discharge passage. Furthermore, as observed from scenario C, the calibrated C_E coefficient was also appropriate to reproduce the erosion pattern of Area 1 (natural channel bed). Thanks to the DoD map the observed erosion pattern was reproduced as a combination of two smoothed slope dependent erosion functions reported in Baggio et al. (2021). For Area 1, where the erosion process resulted less intense, (channel reach upstream of the check dam series) we validated the function C_{Eexp2} (Eq. (5)). Instead for Area 2 (channel reach containing the collapsed check dams) the function C_{Eexp6} (Eq. (4)) represented better the erosion process. Then, it is possible to conclude that the effect of check dam collapse can be calibrated according to the reach erodibility by simulating this intense erosion process similarly to a natural debris-flow channel.

Based on all results, scenario C resulted more precise and then appropriate to simulate check dam collapse than scenario A. However, the simulation setup of scenario A could also be used for check dam collapse simulation, but disregarding real local erosion at the check dam locations and aiming to focus only on the total amount of entrained debris from the channel bed. Accepting this approximation, the simulation setup results easier since it does not require the input on the check dams position and a mask to extract the channel bed area.

The verifications through alternative modelling scenarios also confirmed the outcomes of other studies that highlighted the importance of a careful simulation of debris-flow erosion (Armanini et al., 2009; Gregoretti et al., 2019; Kean et al., 2013). This is always necessary in case the travelling surge suffers a clear modification of its sediment concentration at equilibrium conditions driven by the bed slope, according to Takahashi (2007), or due to the input of supplementary water discharge (e.g. inflow from a tributary branch) or due to the release of supplementary debris (e.g. check dam failure as in our case). For such reasons simulation tools that include the erosion process have to be adopted for the delineation of hazard and risk maps.

In the last decades, attention towards debris-flow structure effectiveness and potential failure consequences has been rising due to their age and lack of maintenance, together with the increasing number of people living in high risk zones (Mazzorana et al., 2014). In particular, different studies pointed out that effectiveness assessment of mitigation structures has to consider potential failures (Chen et al., 2015; Dell'Agnese et al., 2013; Piton et al., 2016). Thanks to our back-

analysis two joint scenarios for the simulation of a check dam series collapse were defined and successfully performed. Other studies investigated the debris flow – check dam interaction. Cui and Chen (2021) and Ferrari et al. (2010) analysed the dam break effect on laboratory experiments and successfully reproduced the observed behaviour with numerical models. Chen et al. (2019) and Marchelli and De Biagi (2019) examined the check dam failure condition and debris-flow surge impacting the check dam through simulation models. Sodnik et al. (2013) proposed a qualitative approach for the evaluation of the hazard level in case of check dam failure. In the mentioned studies some limitations result from the investigation on small scale experiments, the use of single – phase and rigid bed propagation models. The present study, thanks to the availability of a well documented catastrophic event and a specific implementation of the r.avaflow model, overtakes these limitations and it demonstrates a good performance for a complicate real case. The proposed procedure can be directly applied to investigate and assess the potential effects of check dam failure in those torrents where mitigation structures may partially or totally fail. Such a simulation is also capable of driving our decision on maintaining or not ancient check dams in torrents that have been heavily managed in the last centuries (1800 and 1900) and where the erosion control works are in remote wild valleys with difficult access for vehicles and manpower. The results could be used to update the actual debris-flow risk assessment maps (Mazzorana et al., 2009) and help civil authorities in raising residents' awareness of debris-flow events.

5. Conclusions

The study described a catastrophic debris-flow event occurred in the Eastern Italian Alps at the end of the Vaia storm (October 2018). The event was characterized by the collapse of 15 check dams, which destabilized the channel bed. The entrained material increased the debris-flow volume causing sever damages in the fan area. Thanks to the LiDAR and field data, the depositional-erosional pattern of the debris flow was successfully reconstructed. Three complementary different scenarios were implemented to simulate the check dam collapse through bed erosion and mass release. For two of the proposed scenarios, a semi-automatic procedure was developed to calculate the mass release in the case of check dam collapse. The adopted mass flow model r.avaflow resulted particularly suitable for this purpose due to its flexibility in introducing the mass within the computational domain. The observed debris-flow entrainment process in the check dam area mainly occurred through bed erosions rather than released masses. In fact, the total eroded volume resulted five times greater than the estimated volume released by the fifteen check dams (scenario B). The results, together with other companion literature findings, suggest that the effect of check dam failures is often over-estimated as to its power in magnifying the damage. The coefficient of erosion calibrated in Baggio et al. (2021) also resulted suitable to predict the eroded volumes as consequence of check dam failure. This scenario could be immediate to implement for an approximate simulation of the effect of check dam failure.

Summarizing all our findings, we can state that, in the lack of a model capable to simulate check dam collapse and debris flow erosion with a unique simulation, the proposed procedure resulted to be suitable to update the hazard maps in debris-flow channels where mitigation structures are getting old, and to reduce the possible consequences for citizens and infrastructures.

Nomenclature

a, b, c, d	Empirical coefficients for flow velocity estimation
C_E	Coefficient of erosion
C_{Eexp}	Coefficient of erosion derived with exponential function
D	Maximum particle diameter
D_E	Erosion depth
$D_{E,\ max}$	Maximum erosion depth
$_f$	Stands for fluid-phase
H	Flow depth
M	Flow momentum
Q_P	Peak discharge
S	Slope of the thalweg
S_S	Smoothed slope
$_s$	Stands for solid-phase
V	Volume
v	Flow velocity
γ	Flow specific weight
γ_s	Particle specific weight
Δt	Time step length
δu_{pre}	Pre-event DTM error
δu_{post}	Post-event DTM error
δu_{DoD}	Propagated DoD error
$\alpha_{s,\ Emax}$	Solid volumetric concentration of the eroded material

CRediT authorship contribution statement

Tommaso Baggio: Conceptualization, Methodology, Validation, Investigation, Writing - Original Draft.

Vincenzo D'Agostino: Conceptualization, Writing – Review and Editing, Supervision.

Declaration of competing interest

The authors declare that they have no known competing financial interests or personal relationships that could have appeared to influence the work reported in this paper.

Acknowledgements

This research received funding as part of the project “Bridging the mass-flow modelling with the reality”, from the CARIPARO foundation (2724/2018). The study was additionally funded by Provincia Autonoma di Trento through Accordo di Programma GPR. Authors wish to thank the Mountain Basin Service of the Autonomous Province of Trento (IT) for the post-event data and they are also grateful to the three reviewers for their useful suggestions and comments.

References

Armanini, A., 2015. Closure relations for mobile bed debris flows in a wide range of slopes and concentrations. Adv. Water Resour. 81, 75–83. https://doi.org/10.1016/J.ADVWATRES.2014.11.003.

Armanini, A., Fraccarollo, L., Rosatti, G., 2009. Two-dimensional simulation of debris flows in erodible channels. Comput. Geosci. 35, 993–1006. https://doi.org/10.1016/j.cageo.2007.11.008.

Baggio, T., Mergili, M., Pudasaini, S., Carter, S., Fischer, J., 2018. Simulating snow process chains: avalanche-river interactions with r.avaflow. International Snow Science Workshop. Innsbruck, pp. 792–796.

Baggio, T., Mergili, M., D'Agostino, V., 2021. Advances in the simulation of debris flow erosion: the case study of the Rio Gere (Italy) event of the 4th August 2017. Geomorphology 381, 107664. https://doi.org/10.1016/j.geomorph.2021.107664.

Basin Mountain Service, 2018. Post-event Photogrammetric Survey of the rio Rotian (original title, in italian: Rilievo fotogrammetrico post evento del rio Rotian).

Benini, G., 2000. Sistemazioni idraulico forestali. UTET — Unione Tipografico-Editrice Torinese. IT, Torino.

Benito, G., Grodek, T., Enzel, Y., 1998. The geomorphic and hydrologic impacts of the catastrophic failure of flood-control-dams during the 1996-Biescas flood (Central Pyrenees, Spain). Z. Geomorphol. 42, 417–437. https://doi.org/10.1127/zfg/42/1998/417.

Berger, C., McArdell, B.W., Schlunegger, F., 2011. Direct measurement of channel erosion by debris flows, Illgraben, Switzerland. J. Geophys. Res. Earth Surf. 116, n/a-n/a. https://doi.org/10.1029/2010JF001722.

Bernard, M., Boreggio, M., Degetto, M., Gregoretti, C., 2019. Model-based approach for design and performance evaluation of works controlling stony debris flows with an application to a case study at Rovina di Cancia (Venetian Dolomites, Northeast Italy). Sci. Total Environ. 688, 1373–1388. https://doi.org/10.1016/j.scitotenv.2019.05.468.

Berti, M., Genevois, R., LaHusen, R., Simoni, A., Tecca, P.R., 2000. Debris flow monitoring in the acquabona watershed on the Dolomites (Italian alps). Phys. Chem. Earth Part B Hydrol. Oceans Atmos. 25, 707–715. https://doi.org/10.1016/S1464-1909(00)00090-3.

Borga, M., Zaramella, M., 2020. Evento di piena del 27–29 ottobre 2018 sul bacino del Rio Rotian: stima della precipitazione e valutazione della sua severità.
Borga, M., Stoffel, M., Marchi, L., Marra, F., Jakob, M., 2014. Hydrogeomorphic response to extreme rainfall in headwater systems: flash floods and debris flows. J. Hydrol. 518, 194–205. https://doi.org/10.1016/j.jhydrol.2014.05.022.
Brasington, J., Langham, J., Rumsby, B., 2003. Methodological sensitivity of morphometric estimates of coarse fluvial sediment transport. Geomorphology 53, 299–316. https://doi.org/10.1016/S0169-555X(02)00320-3.
Chen, X., Cui, P., You, Y., Chen, J., Li, D., 2015. Engineering measures for debris flow hazard mitigation in the Wenchuan earthquake area. Eng. Geol. 194, 73–85. https://doi.org/10.1016/j.enggeo.2014.10.002.
Chen, H.X., Li, J., Feng, S.J., Gao, H.Y., Zhang, D.M., 2019. Simulation of interactions between debris flow and check dams on three-dimensional terrain. Eng. Geol. 251, 48–62. https://doi.org/10.1016/j.enggeo.2019.02.001.
Chirici, G., Giannetti, F., Travaglini, D., Nocentini, S., Francini, S., D'Amico, G., Calvo, E., Fasolini, D., Broll, M., Maistrelli, F., Tonner, J., Pietrogiovanna, M., Oberlechner, K., Andriolo, A., Comino, R., Faidiga, A., Pasutto, I., Carraro, G., Zen, S., Contarin, F., Alfonsi, L., Wolynski, A., Zanin, M., Gagliano, C., Tonolli, S., Zoanetti, R., Tonetti, R., Cavalli, R., Lingua, E., Pirotti, F., Grigolato, S., Bellingeri, D., Zini, E., Gianelle, D., Dalponte, M., Pompei, E., Stefani, A., Motta, R., Morresi, D., Garbarino, M., Alberti, G., Valdevit, F., Tomelleri, E., Torresani, M., Tonon, G., Marchi, M., Corona, P., Marchetti, M., 2019. Forest damage inventory after the "Vaia" storm in Italy. For. - Riv. di Selvic. ed Ecol. For. 16 (1), 3–9. https://doi.org/10.3832/efor3070-016.
Cucchiaro, S., Cavalli, M., Vericat, D., Crema, S., Llena, M., Beinat, A., Marchi, L., Cazorzi, F., 2019a. Geomorphic effectiveness of check dams in a debris-flow catchment using multi-temporal topographic surveys. Catena 174, 73–83. https://doi.org/10.1016/j.catena.2018.11.004.
Cucchiaro, S., Cazorzi, F., Marchi, L., Crema, S., Beinat, A., Cavalli, M., 2019b. Multi-temporal analysis of the role of check dams in a debris-flow channel: linking structural and functional connectivity. Geomorphology 345, 106844. https://doi.org/10.1016/j.geomorph.2019.106844.
Cui, P., Chen, J., 2021. Numerical simulation of dam-break mudflow based on the Herschel- Bulkley model. EGU, p. 6979.
Dell'Agnese, A., Mazzorana, B., Comiti, F., Von Maravic, P., D'Agostino, V., 2013. Assessing the physical vulnerability of check dams through an empirical damage index. J. Agric. Eng. 44, 9–16. https://doi.org/10.4081/jae.2013.e2.
Dowling, C.A., Santi, P.M., 2014. Debris flows and their toll on human life: a global analysis of debris-flow fatalities from 1950 to 2011. Nat. Hazards 71, 203–227. https://doi.org/10.1007/s11069-013-0907-4.
Ferrari, A., Fraccarollo, L., Dumbser, M., Toro, E.F., Armanini, A., 2010. Three-dimensional flow evolution after a dam break. J. Fluid Mech. 663, 456–477. https://doi.org/10.1017/S0022112010003599.
Frank, F., McArdell, B.W., Huggel, C., Vieli, A., 2015. The importance of entrainment and bulking on debris flow runout modeling: examples from the Swiss Alps. Nat. Hazards Earth Syst. Sci. 15, 2569–2583. https://doi.org/10.5194/nhess-15-2569-2015.
Fuchs, S., Heiss, K., Hübl, J., 2007. Towards an empirical vulnerability function for use in debris flow risk assessment. Nat. Hazards Earth Syst. Sci. 7, 495–506. https://doi.org/10.5194/nhess-7-495-2007.
Gentile, F., Tiziana, A.E., Ae, B., Liuzzi, G.T., 2007. Debris-flow Risk Analysis in South Gargano Watersheds (Southern-Italy). https://doi.org/10.1007/s11069-007-9139-9.
Gong, X.-L., Chen, K.-T., Chen, X.-Q., You, Y., Chen, J.-G., Zhao, W.-Y., Lang, J., 2020. Characteristics of a debris flow disaster and its mitigation countermeasures in Zechawa Gully, Jiuzhaigou Valley, China. Water 12, 25. https://doi.org/10.3390/w12051256.
Gregoretti, C., 2008. Inception sediment transport relationships at high slopes. J. Hydraul. Eng. 134, 1620–1629. https://doi.org/10.1061/(ASCE)0733-9429(2008)134:11(1620).
Gregoretti, C., Degetto, M., Bernard, M., Boreggio, M., 2018. The debris flow occurred at Ru Secco Creek, Venetian Dolomites, on 4 August 2015: analysis of the phenomenon, its characteristics and reproduction by models. Front. Earth Sci. 6, 80. https://doi.org/10.3389/feart.2018.00080.
Gregoretti, C., Stancanelli, L.M., Bernard, M., Boreggio, M., Degetto, M., Lanzoni, S., 2019. Relevance of erosion processes when modelling in channel gravel debris flows for efficient hazard assessment. J. Hydrol. 568, 575–591. https://doi.org/10.1016/j.jhydrol.2018.10.001.
Gylfadóttir, S.S., Mergili, M., Jóhannesson, T., Helgason, J.K., Sæmundsson, Þ., Fischer, J.-T., Pudasaini, S.P., 2019. A Three-Phase Mass Flow Model Applied for the Simulation of Complex Landslide–Glacier–Lake Interactions in Iceland. Geophysical Research Abstracts, in.
Hartmann, S., Pedoth, L., Dalla Torre, C., Schneiderbauer, S., 2021. Beyond the expected-residual risk and cases of overload in the context of managing alpine natural Hazards. Int. J. Disaster Risk Sci. 12, 205–219. https://doi.org/10.1007/s13753-020-00325-3.
Hübl, J., Strauss, A., Holub, M., Suda, J., 2005. Structural mitigation measures. 3rd Probabilistic Workshop: Technical Systems + Natural Hazards. Wien, pp. 115–126.
Huebl, J., Fiebiger, G., 2005. Debris-fow mitigation measures. Debris-Flow Hazards and Related Phenomena. Springer, Berlin, Heidelberg, pp. 445–487.
Hungr, O., Morgan, G.C., Kellerhals, R., 1984. Quantitative analysis of debris torrent hazards for design of remedial measures. Can. Geotech. J. 21, 663–677. https://doi.org/10.1139/t84-073.
Hungr, O., McDougall, S., Bovis, M., 2005. Entrainment of material by debris flows. Debris-Flow Hazards and Related Phenomena. Springer, Berlin, Heidelberg, pp. 135–158 https://doi.org/10.1007/3-540-27129-5_7.
Hungr, O., Leroueil, S., Picarelli, L., 2014. The Varnes classification of landslide types, an update. Landslides 11, 167–194. https://doi.org/10.1007/s10346-013-0436-y.
Jakob, M., Hungr, O., Jakob, D., 2005. Debris-flow Hazards and Related Phenomena. Springer.
Johnson, P.A., McCuen, R.H., 1989. Slit dam design for debris flow mitigation. J. Hydraul. Eng. 115, 1293–1296. https://doi.org/10.1061/(ASCE)0733-9429(1989)115:9(1293).
Kean, J.W., Staley, D.M., Leeper, R.J., Schmidt, K.M., Gartner, J.E., 2012. A low-cost method to measure the timing of postfire flash floods and debris flows relative to rainfall. Water Resour. Res. 48. https://doi.org/10.1029/2011WR011460.
Kean, J.W., McCoy, S.W., Tucker, G.E., Staley, D.M., Coe, J.A., 2013. Runoff-generated debris flows: observations and modeling of surge initiation, magnitude, and frequency. J. Geophys. Res Earth Surf. 118, 2190–2207. https://doi.org/10.1002/jgrf.20148.
Lamb, M.P., Dietrich, W.E., Venditti, J.G., 2008. Is the critical shields stress for incipient sediment motion dependent on channel-bed slope? J. Geophys. Res. Earth Surf. 113, 2008. https://doi.org/10.1029/2007JF000831.
Lanzoni, S., Gregoretti, C., Stancanelli, L.M., 2017. Coarse-grained debris flow dynamics on erodible beds. J. Geophys. Res. Earth Surf. 122, 592–614. https://doi.org/10.1002/2016JF004046.
Larsen, M.C., Wieczorek, G.F., Eaton, L.S., Torres-Sierra, H., 2001. Natural hazards on aluvial fans: the debris flow and flash flood disaster of December 1999, Vargas State, Venezuela. In: Sylva, W. (Ed.), Proceedings of the Sixth Caribbean Islands Water Resources Congress. Mayagüez, Puerto Rico, pp. 1–7.
Liu, J., Nakatani, K., Mizuyama, T., 2012. Effect assessment of debris flow mitigation works based on numerical simulation by using Kanako 2D. Landslides 102 (10), 161–173. https://doi.org/10.1007/S10346-012-0316-X 2012.
Lo, D.O.K., 2000. Review of Natural Terrain Landslide Debris-resisting Barrier Design.
Marchelli, M., De Biagi, V., 2019. Dynamic effects induced by the impact of debris flows on protection barriers. Int. J. Protective Struct. 10, 116–131. https://doi.org/10.1177/2041419618798378.
Marchi, L., Cavalli, M., 2007. Procedures for the documentation of historical debris flows: application to the Chieppena Torrent (Italian Alps). Environ. Manag. 40, 493–503. https://doi.org/10.1007/s00267-006-0288-5.
Marchi, L., D'Agostino, V., 2004. Estimation of debris-flow magnitude in the Eastern Italian Alps. Earth Surf. Process. Landf. 29, 207–220. https://doi.org/10.1002/esp.1027.
Mazzorana, B., Hübl, J., Fuchs, S., 2009. Improving risk assessment by defining consistent and reliable system scenarios. Nat. Hazards Earth Syst. Sci. 9, 145–159. https://doi.org/10.5194/nhess-9-145-2009.
Mazzorana, B., Trenkwalder-Platzer, H.J., Fuchs, S., Hübl, J., 2014. The susceptibility of consolidation check dams as a key factor for maintenance planning. Österr. Wasser Abfallwirtschaft 66, 214–216. https://doi.org/10.1007/s00506-014-0160-4.
McCoy, S.W., Kean, J.W., Coe, J.A., Tucker, G.E., Staley, D.M., Wasklewicz, T.A., 2012. Sediment entrainment by debris flows: in situ measurements from the headwaters of a steep catchment. J. Geophys. Res. Earth Surf. 117, n/a–n/a. https://doi.org/10.1029/2011JF002278.
McDougall, S., Hungr, O., 2004. A model for the analysis of rapid landslide motion across three-dimensional terrain. Can. Geotech. J. 41, 1084–1097. https://doi.org/10.1139/t04-052.
Mergili, M., Pudasaini, S.P., 2021. R.avaflow - the mass flow simulation tool. R.avaflow 2.3 software. URL https://www.avaflow.org. (Accessed 4 December 2021).
Mergili, M., Fischer, J.T., Krenn, J., Pudasaini, S.P., 2017. R.avaflow v1, an advanced open-source computational framework for the propagation and interaction of two-phase mass flows. Geosci. Model Dev. 10, 553–569. https://doi.org/10.5194/gmd-10-553-2017.
Mergili, M., Frank, B., Fischer, J.T., Huggel, C., Pudasaini, S.P., 2018. Computational experiments on the 1962 and 1970 landslide events at Huascarán (Peru) with r.avaflow: lessons learned for predictive mass flow simulations. Geomorphology 322, 15–28. https://doi.org/10.1016/j.geomorph.2018.08.032.
Mergili, M., Mergili, M., Jaboyedoff, M., Pullarello, J., Pudasaini, S.P., 2020a. Back calculation of the 2017 Piz Cengalo-Bondo landslide cascade with r.avaflow: what we can do and what we can learn. Nat. Hazards Earth Syst. Sci. 20, 505–520. https://doi.org/10.5194/nhess-20-505-2020.
Mergili, M., Pudasaini, S.P., Emmer, A., Fischer, J.T., Cochachin, A., Frey, H., 2020b. Reconstruction of the 1941 GLOF process chain at Lake Palcacocha (cordillera Blanca, Peru). Hydrol. Earth Syst. Sci. 24, 93–114. https://doi.org/10.5194/hess-24-93-2020.
Mizuyama, T., 2008. Structural countermeasures for debris flow disasters. Int. J. Erosion Control Eng. 1, 38–43. https://doi.org/10.13101/ijece.1.38.
Mizuyama, T., Kobashi, S., Ou, G., 1992. Prediction of debris flow peak discharge. Interpraevent. Bern, Switzerland, pp. 99–108.
O'Brien, J.S., Julien, P.Y., Fullerton, W.T., 1993. Two-dimensional water flood and mudflow simulation. J. Hydraul. Eng. 119, 244–261. https://doi.org/10.1061/(asce)0733-9429(1993)119:2(244).
Osti, R., Egashira, S., 2008. Method to improve the mitigative effectiveness of a series of check dams against debris flows. Hydrol. Process. 22, 4986–4996. https://doi.org/10.1002/hyp.7118.
Papa, M., Egashira, S., Itoh, T., 2004. Critical conditions of bed sediment entrainment due to debris flow. Nat. Hazards Earth Syst. Sci. 4, 469–474. https://doi.org/10.5194/nhess-4-469-2004.
Piton, G., Recking, A., 2014. The dynamic of streams equipped with Check Dams. River Flow 2014. CRC Press, pp. 1437–1445 https://doi.org/10.1201/b17133-192.
Piton, G., Carladous, S., Recking, A., Tacnet, J.M., Liébault, F., Kuss, D., Quefféléan, Y., Marco, O., 2016. Why do we build check dams in Alpine streams? An historical perspective from the French experience. Earth Surf. Process. Landf. 42, 91–108. https://doi.org/10.1002/esp.3967.
Prein, A.F., Rasmussen, R.M., Ikeda, K., Liu, C., Clark, M.P., Holland, G.J., 2016. The future intensification of hourly precipitation extremes. Nat. Clim. Chang. 7, 48–52. https://doi.org/10.1038/nclimate3168.
Prochaska, A.B., Santi, P.M., Higgins, J.D., Cannon, S.H., 2008. A study of methods to estimate debris flow velocity. Landslides 5, 431–444. https://doi.org/10.1007/s10346-008-0137-0.

Pudasaini, S.P., Mergili, M., 2019. A multi-phase mass flow model. J. Geophys. Res. Earth Surf. 124, 1–23. https://doi.org/10.1029/2019jf005204.

Remaître, A., Van Asch T., W.J., Malet, J.P., Maquaire, O., 2008. Influence of check dams on debris-flow run-out intensity. Nat. Hazards Earth Syst. Sci. 8, 1403–1416. https://doi.org/10.5194/nhess-8-1403-2008.

Rickenmann, D., 1999. Empirical relationships for debris flow. Nat. Hazards 19, 47–77.

Rickenmann, D., Zimmermann, M., 1993. The 1987 debris flows in Switzerland: documentation and analysis. Geomorphology 8, 175–189. https://doi.org/10.1016/0169-555X(93)90036-2.

Rickenmann, D., Weber, D., Stepanov, B., 2003. Erosion by debris flows in field and laboratory experiments. International Conference on Debris-Flow Hazards Mitigation: Mechanics, Prediction, and Assessment, Proceedings. 2, pp. 883–894.

Rodríguez-Morata, C., Villacorta, S., Stoffel, M., Ballesteros-Cánovas, J.A., 2019. Assessing strategies to mitigate debris-flow risk in Abancay province, south-central Peruvian Andes. Geomorphology 342, 127–139. https://doi.org/10.1016/j.geomorph.2019.06.012.

Rosatti, G., Begnudelli, L., 2013. Two-dimensional simulation of debris flows over mobile bed: enhancing the TRENT2D model by using a well-balanced generalized roe-type solver. Computers Fluids 71, 179–195. https://doi.org/10.1016/j.compfluid.2012.10.006.

Scheidl, C., Rickenmann, D., McArdell, B.W., 2013. Runout prediction of debris flows and similar mass movements. Landslide Science and Practice. Springer, Berlin Heidelberg, pp. 221–229 https://doi.org/10.1007/978-3-642-31310-3_30.

Simoni, A., Bernard, M., Berti, M., Boreggio, M., Lanzoni, S., Stancanelli, L.M., Gregoretti, C., 2020. Runoff-generated debris flows: observation of initiation conditions and erosion–deposition dynamics along the channel at Cancia (eastern Italian Alps). Earth Surf. Process. Landf. 45, 3556–3571. https://doi.org/10.1002/esp.4981.

Sodnik, J., Kryžanowski, A., Martin, M., Mikoš, M., 2013. Torrential check dams as debris-flow sources. Landslide and Flood Hazard Assessment. Zagreb, pp. 6–9.

Stecher, M., Mazzorana, B., Hübl, J., 2012. Proposal of risk mitigation strategies based on a conceptual planning approach. A case study conducted in the Gadriabach study site, Vinschgau valley, Italy. Interpraevent. Grenoble, pp. 811–820.

Stoffel, M., Tiranti, D., Huggel, C., 2014. Climate change impacts on mass movements - case studies from the European Alps. Sci. Total Environ. 493, 1255–1266. https://doi.org/10.1016/j.scitotenv.2014.02.102.

Tacnet, J.-M., Curt, C., Benjamin, R., Richard, D., 2012. Efficiency assessment for torrent protection works. Interpraevent. Grenoble, pp. 821–831.

Takahashi, T., 2007. Debris Flow: Mechanics. Taylor & Francis, Prediction and Countermeasures.

Tseng, W.H., Wang, H.W., Chou, S.C., Kao, Y.L., Shieh, C.L., 2012. Experiments on channel evolution caused by check-dam failure. J. Mt. Sci. 9, 175–184. https://doi.org/10.1007/s11629-012-2252-6.

Vagnon, F., 2020. Design of active debris flow mitigation measures: a comprehensive analysis of existing impact models. Landslides 17, 313–333. https://doi.org/10.1007/s10346-019-01278-5.

Victoriano, A., Brasington, J., Guinau, M., Furdada, G., Cabré, M., Moysset, M., 2018. Geomorphic impact and assessment of flexible barriers using multi-temporal LiDAR data: the Portainé mountain catchment (Pyrenees). Eng. Geol. 237, 168–180. https://doi.org/10.1016/j.enggeo.2018.02.016.

Wang, G.L., 2013. Lessons learned from protective measures associated with the 2010 Zhouqu debris flow disaster in China. Nat. Hazards 69, 1835–1847. https://doi.org/10.1007/s11069-013-0772-1.

Zeng, Q.L., Yue, Z.Q., Yang, Z.F., Zhang, X.J., 2009. A case study of long-term field performance of check-dams in mitigation of soil erosion in Jiangjia stream, China. Environ. Geol. 58, 897–911. https://doi.org/10.1007/s00254-008-1570-z.

Zhang, F., Yan, B., Feng, X., Lan, H., Kang, C., Lin, X., Zhu, X., Ma, W., 2019. A rapid loess mudflow triggered by the check dam failure in a bulldoze mountain area, Lanzhou, China. Landslides 16, 1981–1992. https://doi.org/10.1007/s10346-019-01219-2.